

# Coulomb excitation of the $|T_z| = \frac{1}{2}$ , $A = 23$ mirror pair and systematics of *ab-initio* $E2$ strength

J. Henderson,<sup>1,2,\*</sup> G. Hackman,<sup>1</sup> P. Ruotsalainen,<sup>3</sup> J. D. Holt,<sup>1,4</sup> S. R. Stroberg,<sup>1,5</sup> G. Hagen,<sup>6,7,1</sup> C. Andreoiu,<sup>8</sup> G. C. Ball,<sup>1</sup> N. Bernier,<sup>1,9,†</sup> M. Bowry,<sup>1,‡</sup> R. Caballero-Folch,<sup>1</sup> S. Cruz,<sup>1,9</sup> A. Diaz Varela,<sup>10</sup> L. J. Evitts,<sup>1,11,§</sup> R. Frederick,<sup>1</sup> A. B. Garnsworthy,<sup>1</sup> M. Holl,<sup>12,1,¶</sup> J. Lassen,<sup>1</sup> J. Measures,<sup>1,11</sup> B. Olaizola,<sup>1</sup> E. O’Sullivan,<sup>1</sup> O. Paetkau,<sup>1</sup> J. Park,<sup>1,9,\*\*</sup> J. Smallcombe,<sup>1,††</sup> C. E. Svensson,<sup>10</sup> K. Whitmore,<sup>8</sup> and C. Y. Wu<sup>2</sup>

<sup>1</sup>TRIUMF, Vancouver, BC V6T 2A3, Canada

<sup>2</sup>Lawrence Livermore National Laboratory, Livermore, CA 94550, USA

<sup>3</sup>University of Jyväskylä, Department of Physics,

P. O. Box 35, FI-40014 University of Jyväskylä, Finland

<sup>4</sup>Department of Physics, McGill University, 3600 Rue University, Montréal, QC H3A 2T8, Canada

<sup>5</sup>Department of Physics, University of Washington, Seattle WA, USA

<sup>6</sup>Physics Division, Oak Ridge National Laboratory, Oak Ridge, Tennessee 37831, USA

<sup>7</sup>Department of Physics and Astronomy, University of Tennessee, Knoxville, Tennessee 37996, USA

<sup>8</sup>Department of Chemistry, Simon Fraser University, Burnaby, BC V5A 1S6, Canada

<sup>9</sup>Department of Physics and Astronomy, University of British Columbia, Vancouver V6T 1Z1, Canada

<sup>10</sup>Department of Physics, University of Guelph, Guelph, ON N1G 2W1, Canada

<sup>11</sup>Department of Physics, University of Surrey, Guildford, GU2 7XH, United Kingdom

<sup>12</sup>Department of Astronomy and Physics, Saint Mary’s University, Halifax, Nova Scotia B3H 3C3, Canada

(Dated: May 11, 2020)

**Background:** Recent developments in *ab initio* nuclear theory demonstrate promising results in medium- to heavy-mass nuclei. A particular challenge for many of the many-body methodologies, however, is an accurate treatment of the electric-quadrupole,  $E2$ , strength associated with collectivity.

**Purpose:** In this work we present high-precision  $E2$  data for the mirror nuclei  $^{23}\text{Mg}$  and  $^{23}\text{Na}$  for comparison with such theory. We interpret these results in combination with other recent measurements performed by the collaboration and the available literature.

**Methods:** Coulomb-excitation measurements of  $^{23}\text{Mg}$  and  $^{23}\text{Na}$  were performed at the TRIUMF-ISAC facility using the TIGRESS spectrometer and were used to determine the  $E2$  matrix elements of mixed  $E2/M1$  transitions.

**Results:**  $E2$  transition strengths were extracted for  $^{23}\text{Mg}$  and  $^{23}\text{Na}$ . Transition strength ( $B(E2)$ ) precision was improved by factors of approximately six for both isotopes, while agreeing within uncertainties with previous measurements.

**Conclusions:** A comparison was made with both shell-model and *ab initio* valence-space in-medium similarity renormalization group calculations. Valence-Space In-Medium Similarity-Renormalization-Group calculations were found to underpredict the absolute  $E2$  strength - in agreement with previous results - but a full analysis of *sd*-shell nuclei found no indication of an isovector component to the missing strength. Comparison with full configuration interaction and coupled cluster calculations in the case of  $^{14}\text{C}$  indicates that correlated multi-particle multi-hole excitations are essential to the reproduction of quadrupole excitation amplitudes.

## I. INTRODUCTION

The strength of electric quadrupole ( $E2$ ) transitions between excited states in nuclei is closely related to the bulk, collective motion of nucleons arising from devia-

tions of the nucleus from sphericity. The theoretical reproduction of this  $E2$  strength has long been problematic for traditional microscopic nuclear methodologies, such as the phenomenological nuclear shell model. The shell model begins with a spherical potential, and collectivity has therefore to be introduced through multi-particle multi-hole (mp-mh) excitations, with large contributions from configurations outside the shell-model, or valence, space. In a recent work [1], we investigated the ability of modern, microscopically derived nuclear theory to reproduce  $E2$  strength without the use of adjustments to the nucleon charges (*effective charges*) that are required in traditional methodologies. It was found that the symplectic no-core shell model (NCSpM) reproduced the experimental data well using an appropriate subset of mp-mh excitations to account for the collective motion of the nucleons. *Ab initio* valence-space in-medium similarity renormalization group (VS-IMSRG) calculations mean-

\* henderson64@llnl.gov

† Present Address: Department of Physics & Astronomy, University of the Western Cape, Bellville-7535, South Africa

‡ Present address: University of the West of Scotland, United Kingdom

§ Present address: School of Computer Science and Electronic Engineering, Bangor University, Bangor, Gwynedd, LL57 2DG, UK

¶ Present address: Department of Physics, Chalmers University of Technology, SE-412 96 Göteborg, Sweden

\*\* Present address: Center for Exotic Nuclear Studies, Institute for Basic Science (IBS), Daejeon 34126, Republic of Korea

†† Present address: Oliver Lodge Laboratory, University of Liverpool, Liverpool L69 7ZE, United Kingdom

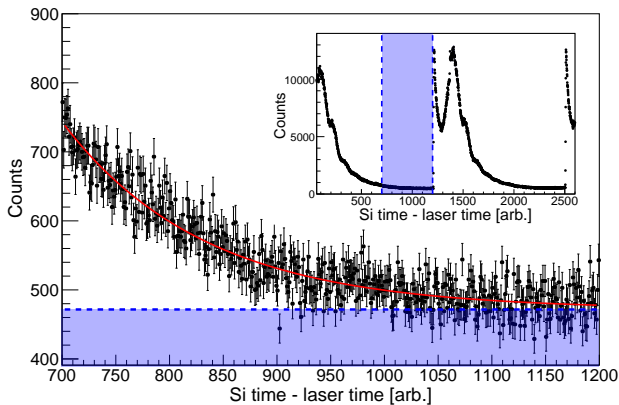


FIG. 1. Tail of the silicon-time laser-time distribution (see text for details), fit with an exponential plus constant background. The integral of the background is used to determine the surface ionized contamination originating from  $^{23}\text{Na}$ . Shown in the inset is the total time structure arising from the laser-ionization in the present measurement with the fitted area indicated.

while failed to reproduce the absolute  $E2$  strength but provided superior qualitative description of the experimental evolution of  $E2$  strength in the  $sd$ -shell, as compared to phenomenological shell-model calculations. In order to assess this further, a wider study of the  $sd$ -shell is warranted, with further requirements for improved data around the  $N = Z$  line.

The precision to which  $E2$  strengths are determined in odd-mass  $sd$ -shell nuclei is often limited by the fact that decays are of a mixed  $E2/M1$  nature. When the decay is dominated by  $M1$  strength, as is the case in  $^{23}\text{Mg}$  and  $^{23}\text{Na}$ , the leading uncertainty in determining the  $E2$  strength is typically the mixing ratio  $\delta$  between  $E2$  and  $M1$  contributions determined, for example, from the angular correlations between emitted  $\gamma$  rays. By performing a Coulomb excitation measurement, rather than determining the  $E2$  strength from the decay properties, this source of uncertainty can be largely eliminated, allowing for a higher level of precision. We therefore report on two Coulomb excitation measurements of radioactive  $^{23}\text{Mg}$  and stable  $^{23}\text{Na}$ , with the goal of determining precise  $E2$  matrix elements for comparison with state-of-the-art nuclear theory.

## II. EXPERIMENTAL DETAILS

$^{23}\text{Mg}$  and  $^{23}\text{Na}$  were investigated through Coulomb excitation using the TIGRESS facility [2] at TRIUMF ISAC.  $^{23}\text{Mg}$  nuclei were produced by the impinging of 480-MeV protons onto a SiC ISAC target. The Mg atoms produced were then selectively laser ionized using three step resonant excitation (285.3 nm-880.8 nm-291.6 nm) into an auto-ionizing state and extracted.  $^{23}\text{Na}$  contamination was suppressed by the use of the ion-guide laser ion source (IG-LIS) [3]. A repeller plate is held at

40 V to suppress the extraction of surface-ionized contaminants by factors of up to  $10^6$ .  $^{23}\text{Na}$  ions were produced by the surface ion source of the TRIUMF offline ion source (OLIS) [4]. The beams were then accelerated by the TRIUMF ISAC accelerator chain and delivered to TIGRESS. The  $^{23}\text{Mg}/^{23}\text{Na}$  cocktail beam was delivered at an energy of 42.9 MeV, while the  $^{23}\text{Na}$  beam provided by OLIS was delivered energies of both 42.9 MeV and 39.4 MeV. The total beam intensity delivered to TIGRESS for the  $^{23}\text{Mg}$  portion of the experiment was maintained at roughly  $3 \cdot 10^5$  particles per second - this includes a component from the remaining  $^{23}\text{Na}$  contamination. The  $^{23}\text{Na}$  beam intensity was maintained at approximately  $6 \cdot 10^7$  particles per second. The beams were then impinged onto a 0.44-mg/cm<sup>2</sup> thick,  $^{nat}\text{Ti}$  target at the center of the TIGRESS array. Scattered beam- and target-like nuclei were detected in an S3-type silicon detector, mounted 31-mm downstream of the target position within the BAMBINO target chamber. Gamma rays were detected using the TIGRESS array, which for the present measurement comprised fourteen clover-type HPGe detectors. The HPGe detectors were operated in their withdrawn configuration, with the face of the detectors 14.5 cm from the target and the BGO suppression shields forward, providing the best possible peak-to-background ratio and Doppler-correction.

While the use of IG-LIS heavily suppresses extraction of  $^{23}\text{Na}$ , a degree of contamination remains which was monitored in two ways. First, a Bragg detector was used to provide an instantaneous measure of the beam composition. While the composition is being determined in this way experimental data cannot be acquired. For the second method, the 10 kHz signal used to synchronize the laser ionization system was used, with every second pulse triggering the generation of a ramping waveform, which could then be digitized. The amplitude of the digitized waveform thereby gave a proxy for the time of the detection relative to the laser-ionization pulse and could thus be used to distinguish laser-ionized beam components which had a 10 kHz pulsed structure from the continuous surface ionized contaminants. This method allowed for a continuous determination of contamination, allowing to monitor for sudden changes in the ISAC target behavior. Based on these analyses, the  $^{23}\text{Na}$  contribution to the beam cocktail was determined to be 15.2(9) % of the total, with the uncertainty being predominantly systematic and arising from the choice of fitting region. Figure 1 shows the laser timing distribution, the tail of which was fit with an exponential and baseline to determine the relative contributions to the beam cocktail.

## III. ANALYSIS

The data were unpacked using the GRSISort [5] software package, built in a ROOT [6] framework. Gamma-ray events were Doppler corrected event-by-event on the basis of the beam and target kinematics determined from

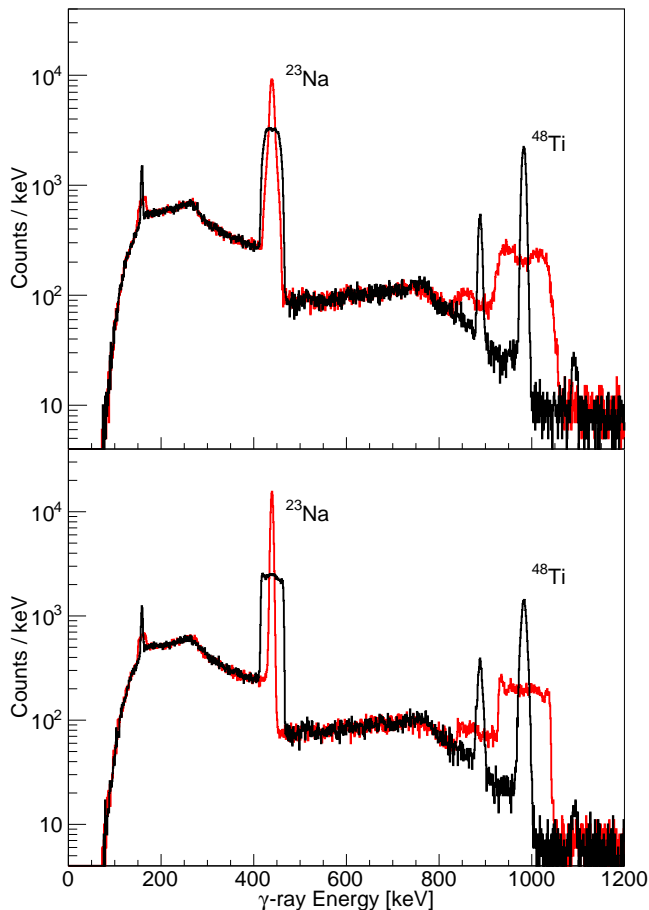


FIG. 2. Doppler-corrected  $\gamma$ -ray spectra on the basis of  $^{23}\text{Na}$  (red) and  $^{48}\text{Ti}$  (black) kinematics for a  $^{23}\text{Na}$  beam energy of 39.4 MeV. Top: Detection of a target-like recoil ( $^{48}\text{Ti}$ ) in the downstream annular silicon detector. Bottom: Detection of a beam-like recoil ( $^{23}\text{Na}$ ) in the downstream annular silicon detector. The additional width of the  $^{23}\text{Na}$  peak in the top figure arises from the wide angles at which the scattering occurs, leading to significant slowing in the target material. Other lines in the titanium corrected (black) spectra arise from isotopes of titanium with a lower natural abundance than  $^{48}\text{Ti}$  (73.8%).

the hit location in the annular silicon detectors and whether the detected particle had beam-like or target-like kinematic properties. Gamma-ray spectra for  $^{23}\text{Na}$  at 39.4 MeV, and the  $^{23}\text{Mg} + ^{23}\text{Na}$  cocktail beam are shown in Fig. 2 and Fig. 3, respectively. Relative  $\gamma$ -ray detection efficiencies for TIGRESS were determined using a standard suite of  $^{152}\text{Eu}$ ,  $^{133}\text{Ba}$  and  $^{60}\text{Co}$  sources.  $^{23}\text{Na}$  data were split into forty-eight groups: twelve angular bins for both beam-like and target-like detection, repeated for both beam energies. The  $^{23}\text{Mg}$  data were binned in twelve groups, six angular groups each for beam-like and target-like scattering. Yields were adjusted for the natural abundance of  $^{48}\text{Ti}$ .

In the beam-like scattering data the  $^{23}\text{Mg}$  and  $^{23}\text{Na}$   $\gamma$ -ray lines were readily distinguished and were fitted in-

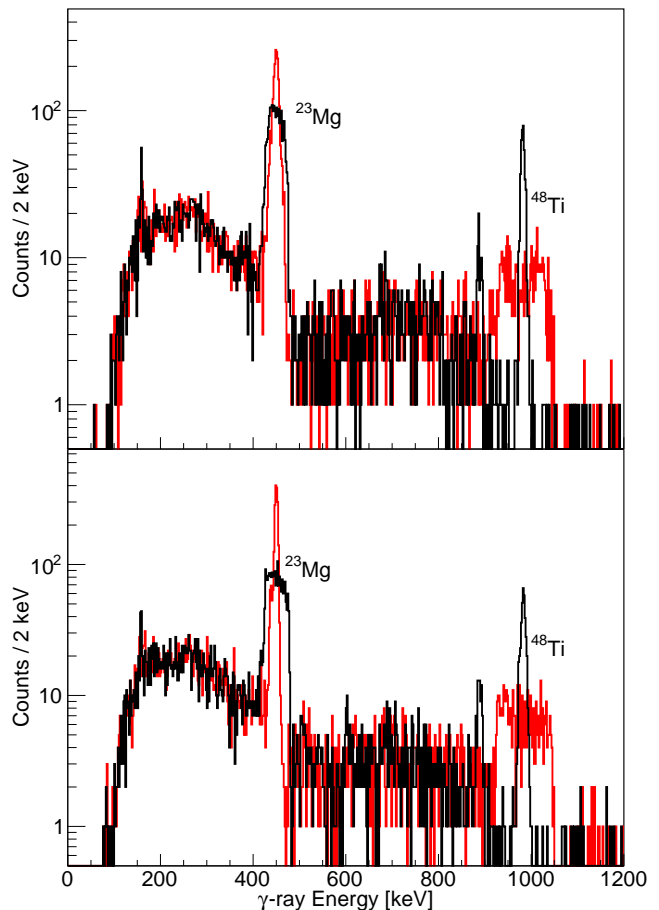


FIG. 3. As Fig. 2 but for a cocktail  $^{23}\text{Mg}$  ( $\sim 85\%$ ) and  $^{23}\text{Na}$  ( $\sim 15\%$ ) beam at an energy of 42.9 MeV.

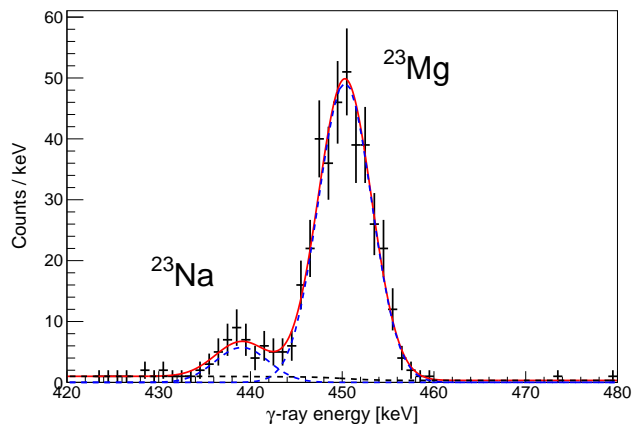


FIG. 4. Fit of the  $\gamma$ -ray peaks observed in TIGRESS corresponding to the de-excitation of the first-excited state in  $^{23}\text{Mg}$  and the analogue state in the stable contaminant and mirror nucleus,  $^{23}\text{Na}$ . These data were coincident with events from the first four rings of the downstream annular silicon detector, corresponding to angles of  $19.5^\circ \rightarrow 25.8^\circ$ . This fitting method can be used for all cases where the beam-like particle was detected. See the text for details of the analysis for target-like particle detection.

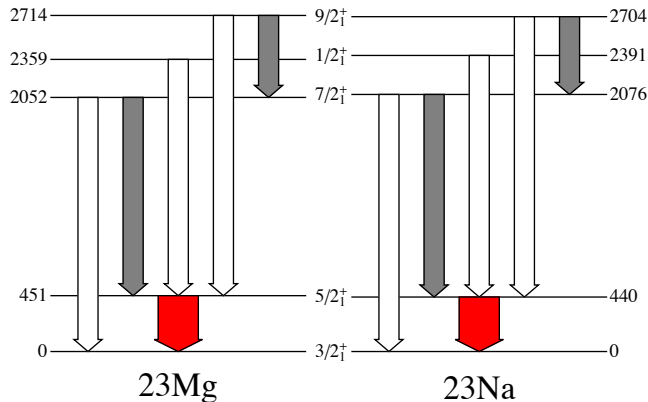


FIG. 5. Low-lying levels in  $^{23}\text{Mg}$  and  $^{23}\text{Na}$  relevant to the present analysis. The  $5/2^+ \rightarrow 3/2^+$  transition (red) was investigated and other transitions were included within the GOSIA analysis. Gray transitions indicate mixed  $E2/M1$ .

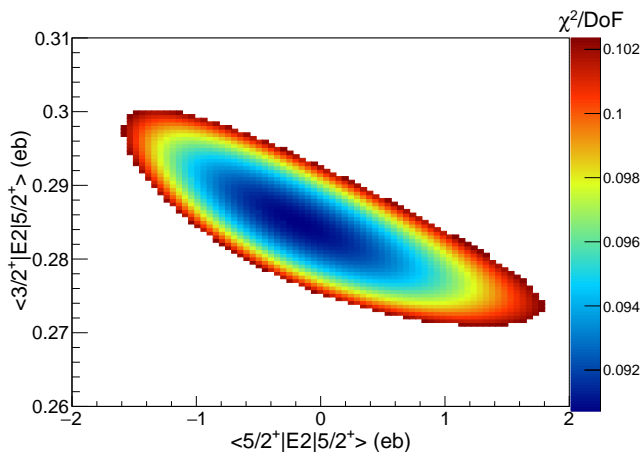


FIG. 6.  $\chi^2$  surface resulting from the GOSIA2 analysis of  $^{23}\text{Mg}$  from which transition and diagonal matrix-elements were extracted.

dividually, as shown in Fig. 4. The observed  $^{48}\text{Ti}$  yield was then adjusted for the observed  $^{23}\text{Na}$  component on the basis of the 42.9 MeV  $^{23}\text{Na}$  data. For the target scattering data the two components of the  $A = 23$   $\gamma$ -ray peak were not always distinguishable. The  $^{23}\text{Na}$  component was therefore determined and subtracted on the basis of the observed component in the beam-like scattering data and of the 42.9 MeV, pure (OLIS)  $^{23}\text{Na}$  data.  $^{23}\text{Na}$  contamination could thereby be handled empirically, without requiring assumptions about beam composition and minimizing the introduction of systematic uncertainties.

The Coulomb-excitation analysis was performed in the coupled-channels GOSIA2 code [7] used to simultaneously analyze beam- and target-like data. The levels included in the GOSIA2 analysis are shown in

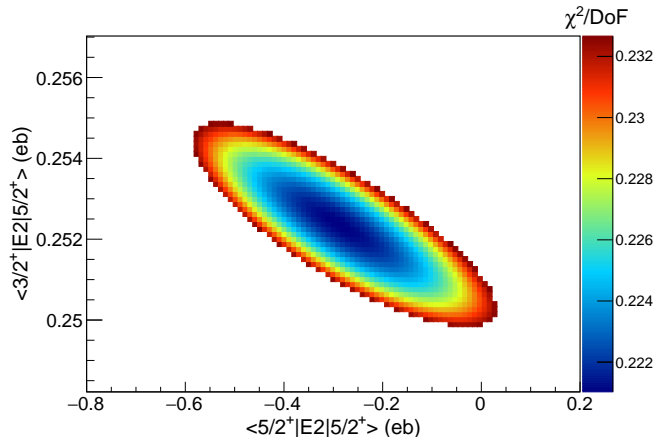


FIG. 7.  $\chi^2$  surface resulting from the GOSIA2 analysis of  $^{23}\text{Na}$  from which transition and diagonal matrix-elements were extracted.

Fig. 5. Ground-state spectroscopic quadrupole moments for both  $^{23}\text{Na}$  and  $^{23}\text{Mg}$  were taken at their literature values [8]. For each beam all data were analyzed simultaneously, maximizing sensitivity. The  $\langle \frac{3}{2}^+ | E2 | \frac{5}{2}^+ \rangle$  and  $\langle \frac{5}{2}^+ | E2 | \frac{5}{2}^+ \rangle$  matrix elements were varied in order to construct  $\chi^2$  surfaces to incorporate any mutual dependence.  $\chi^2$  surfaces for  $^{23}\text{Mg}$  and  $^{23}\text{Na}$  are shown in Fig. 6 and Fig. 7, respectively. Little sensitivity was found to the diagonal matrix element beyond an indication of the sign in  $^{23}\text{Na}$ . Matrix elements to higher-lying states were fixed to their literature values during the minimization procedure, however their  $1\sigma$  limits were investigated to quantify any impact on the result and are incorporated as a systematic uncertainty. Extracted matrix elements are summarized in Tab. I, along with other properties derived from the present results.

#### IV. DISCUSSION

The  $B(E2)$  values extracted in the present work are presented in Table II, along with the present state of knowledge for  $T_z = \pm \frac{1}{2}$  nuclei with  $19 \leq A \leq 31$ . Also shown are the results of calculations using the *ab initio* VS-IMSRG methodology [10–13], with a consistently evolved valence-space  $E2$  operator which does not rely on the use of any effective charges. The VS-IMSRG calculations were performed using the EM1.8/2.0 interaction [14, 15], which was generated by SRG evolution [16] of the chiral  $\text{N}^3\text{LO}$  NN interaction of Entem and Machleidt [17], and adding a non-locally regulated  $\text{N}^2\text{LO}$  3N interaction with the low energy constants adjusted to reproduce the triton binding energy and the  $^4\text{He}$  matter radius. While only constrained with  $A \leq 4$  data, this interaction gives a remarkable reproduction of binding energies and spectroscopy up to at least  $A \sim 100$ , with a general underprediction of radii [18–20]. Cal-

TABLE I.  $E2$  matrix elements,  $B(E2)$  values, spectroscopic quadrupole moments and mixing ratios deduced from the present work with statistical and systematic uncertainties quoted. Where available, literature values are shown for comparison. Mixing ratios were deduced on the basis of the literature lifetimes and the presently determined  $B(E2)$  values.

$^{23}\text{Na}$	This Work	Literature	Ref.
$\langle \frac{3}{2}^+   E2   \frac{5}{2}^+ \rangle$ eb	0.252(3)(4)	0.237 ( $\frac{14}{15}$ )	[9]
$B(E2; \frac{5}{2}^+ \rightarrow \frac{3}{2}^+)$ e $^2\text{fm}^4$	106 (3) (3)	93 (12)	[9]
$\langle \frac{5}{2}^+   E2   \frac{5}{2}^+ \rangle$ eb	-0.29 ( $\frac{32}{29}$ ) (5)		
$Q_s(\frac{5}{2}^+)$ eb	-0.22 ( $\frac{25}{22}$ ) (4)		
$\delta_{E2/M1}^2$	0.0038(4)	0.0034(2)	[9]
$^{23}\text{Mg}$			
$\langle \frac{3}{2}^+   E2   \frac{5}{2}^+ \rangle$ eb	0.285 (15) (4)	0.23 ( $\frac{7}{10}$ )	[9]
$B(E2; \frac{5}{2}^+ \rightarrow \frac{3}{2}^+)$ e $^2\text{fm}^4$	135 ( $\frac{15}{14}$ ) (4)	86 (58)	[9]
$\langle \frac{5}{2}^+   E2   \frac{5}{2}^+ \rangle$ eb	-0.2 ( $\frac{20}{13}$ )		
$Q_s(\frac{5}{2}^+)$ eb	-0.15 ( $\frac{150}{100}$ )		
$\delta_{E2/M1}^2$	0.0056(6)	0.0036(12)	[9]

calculations are performed in a harmonic oscillator basis of  $\hbar\omega = 20$  MeV with  $2n + \ell \leq e_{max}=12$  and an additional truncation on the three body matrix elements  $e_1 + e_2 + e_3 \leq E_{3max}=16$ . Following a Hartree-Fock calculation, all operators are truncated at the normal-ordered two-body level. Also shown are shell-model calculations performed with the USDB interaction [21]. In both cases, shell model diagonalizations are performed using the code NuShellX [22], and the transition densities needed for the VS-IMSRG operators are computed using the nutbar code [23]. The nominal USDB effective charges of  $e^\pi = 1.36$  and  $e^\nu = 0.45$  were used for all phenomenological shell-model calculations. Shown in Table III are  $T_z = \pm 1$  nuclei, in Table IV are  $T_z = \pm \frac{3}{2}$  nuclei and in Table V  $T_z = \pm 2$  nuclei.

The experimental and calculated values for  $|T_z| = \frac{1}{2}$ ,  $|T_z| = 1$  and  $|T_z| = 2$  are shown in Fig 8, Fig 9 and Fig 10, respectively. Due to the limited available experimental data, values for  $T_z = \frac{3}{2}$  are not plotted here, but a similar plot can be found in Ref. [24]. Clearly, from the results presented in Tables. II to V and Figures 8 to 10, the VS-IMSRG calculations underpredict absolute  $B(E2)$  strength, as was previously reported [1, 24]. As would be expected, the USDB calculations with nominal effective charges reproduce the absolute strength relatively well.

In order to understand the nature of the missing strength in the VS-IMSRG calculations, it bears briefly summarizing the many-body method. An approximately unitary transformation is performed on the Hamiltonian in the large Hilbert space (here 13 major oscillator shells) so as to decouple a tractable valence space - analogous to a shell-model space - from the full space. The result is an effective Hamiltonian in which couplings to excitations out of the valence space are suppressed. The

TABLE II.  $B(E2)$  values for transitions between the ground and first-excited states in  $|T_z = \frac{1}{2}|$  nuclei in the  $sd$  shell, comparing experimental values with those calculated using VS-IMSRG with the EM1.8/2.0 interaction and with the USDB shell-model interaction. Shell-model calculations used effective charges of  $e^\pi = 1.36$  and  $e^\nu = 0.45$ .

Isotope	$J_i^\pi$	$J_f^\pi$	B(E2) $\downarrow$ [e $^2\text{fm}^4$ ]			
			Expt.	VS-IMSRG	USDB	Ref. (Expt.)
$^{19}\text{Ne}$	$\frac{5}{2}^+$	$\frac{1}{2}^+$	39.8 (15)	25.0	36.9	[9]
$^{19}\text{F}$	$\frac{5}{2}^+$	$\frac{1}{2}^+$	20.9 (2)	9.8	19.4	[9]
$^{21}\text{Na}$	$\frac{5}{2}^+$	$\frac{3}{2}^+$	136.5 (92)	56.1	90.2	[9]
$^{21}\text{Ne}$	$\frac{5}{2}^+$	$\frac{3}{2}^+$	87.5 (58)	39.1	76.1	[9]
$^{23}\text{Mg}$	$\frac{5}{2}^+$	$\frac{3}{2}^+$	135 (15)	75.2	117.3	This Work
$^{23}\text{Na}$	$\frac{5}{2}^+$	$\frac{3}{2}^+$	106 (4)	56.9	109.1	This Work
$^{25}\text{Al}$	$\frac{1}{2}^+$	$\frac{5}{2}^+$	13.2 (3)	7.6	3.8	[9]
$^{25}\text{Mg}$	$\frac{1}{2}^+$	$\frac{5}{2}^+$	2.44 (4)	1.09	3.03	[9]
$^{27}\text{Si}$	$\frac{1}{2}^+$	$\frac{5}{2}^+$	55.7 (64)	58.2	81.0	[9]
$^{27}\text{Al}$	$\frac{1}{2}^+$	$\frac{5}{2}^+$	37.8 (11)	38.1	54.6	[9]
$^{29}\text{P}$	$\frac{3}{2}^+$	$\frac{1}{2}^+$	21.7 (21)	17.2	45.8	[9]
$^{29}\text{Si}$	$\frac{3}{2}^+$	$\frac{1}{2}^+$	14.3 (27)	7.4	31.0	[9]
$^{31}\text{S}$	$\frac{3}{2}^+$	$\frac{1}{2}^+$	40.5 (116)	24.1	39.6	[9]
$^{31}\text{P}$	$\frac{3}{2}^+$	$\frac{1}{2}^+$	24.3 (35)	16.7	35.2	[9]
$^{31}\text{S}$	$\frac{5}{2}^+$	$\frac{1}{2}^+$	45.1 (127)	28.7	46.8	[9]
$^{31}\text{P}$	$\frac{5}{2}^+$	$\frac{1}{2}^+$	37.0 (29)	23.3	44.4	[9]

TABLE III. As Table II but for  $|T_z = 1|$  nuclei.

Isotope	Expt.	B(E2) $\downarrow$ [e $^2\text{fm}^4$ ]			Ref. (Expt.)
		VS-IMSRG	USDB		
$^{18}\text{Ne}$	49.6 (50)	19.0	29.8		[9]
$^{18}\text{O}$	9.3 (3)	0.7	3.3		[9]
$^{22}\text{Mg}$	76.2 (92)	45.0	65.8		[1]
$^{22}\text{Ne}$	46.9 (5)	22.7	49.0		[1, 9] $^\dagger$
$^{26}\text{Si}$	70.0 (69)	45.6	47.1		[9]
$^{26}\text{Mg}$	61.3 (26)	36.2	69.0		[9]
$^{30}\text{S}$	68.7 (40)	42.0	59.5		[9]
$^{30}\text{Si}$	49.9 (65)	24.4	48.0		[9]
$^{34}\text{Ar}$	44.5 (59)	30.6	46.3		[9]
$^{34}\text{S}$	40.8 (11)	24.9	37.6		[9]

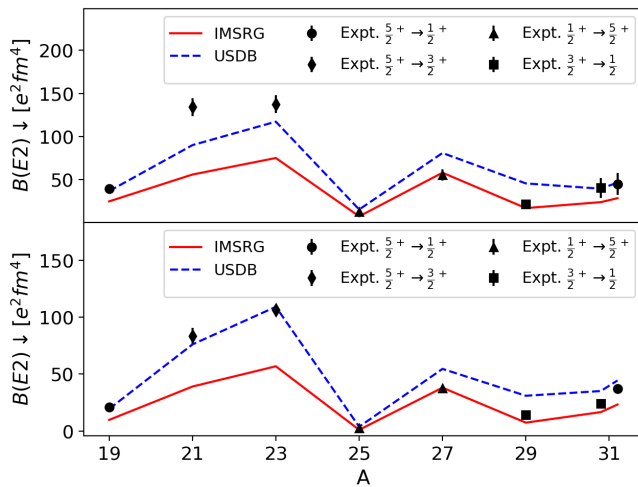
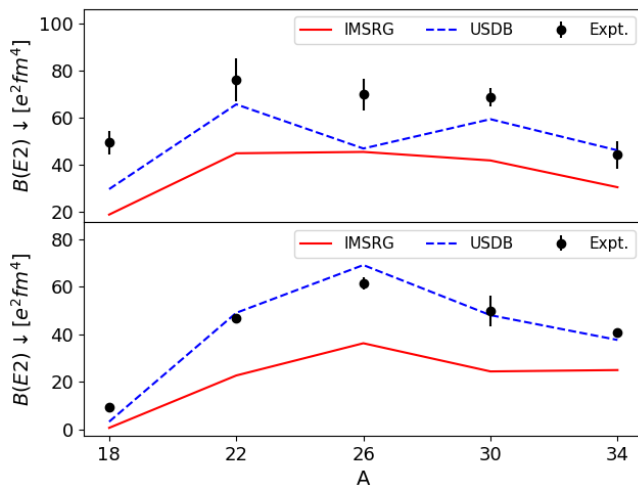
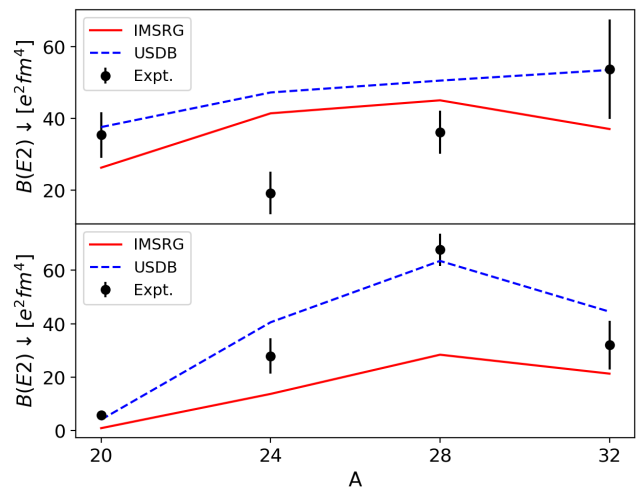
$^\dagger$  - Weighted average of values in Ref. [1] and Ref. [9]

TABLE IV. As Table II but for  $|T_z = \frac{3}{2}|$  nuclei.

Isotope	$J_i^\pi$	$J_f^\pi$	B(E2) $\downarrow$ [e $^2\text{fm}^4$ ]			
			Expt.	VS-IMSRG	USDB	Ref. (Expt.)
$^{21}\text{Mg}$	$\frac{1}{2}^+$	$\frac{5}{2}^+$	131.1 (14)	94.6	132.0	[24]
$^{21}\text{F}$	$\frac{1}{2}^+$	$\frac{5}{2}^+$	54.0 ( 55)	23.6	60.5	[25]
$^{21}\text{Mg}$	$\frac{9}{2}^+$	$\frac{5}{2}^+$	83.7 (140)	21.3	55.6	[24]
$^{21}\text{F}$	$\frac{9}{2}^+$	$\frac{5}{2}^+$	14.3 (21)	6.4	16.8	[25]
$^{33}\text{Ar}$	$\frac{3}{2}^+$	$\frac{1}{2}^+$	40.2 (94)	19.8	33.6	[9]
$^{33}\text{P}$	$\frac{3}{2}^+$	$\frac{1}{2}^+$	62.9 (252)	18.6	39.7	[9]
$^{33}\text{Ar}$	$\frac{5}{2}^+$	$\frac{1}{2}^+$	36.5 (101)	25.4	45.4	[9]
$^{33}\text{P}$	$\frac{5}{2}^+$	$\frac{1}{2}^+$	32.1 (50)	13.6	31.5	[9]

TABLE V. As Table II but for  $|T_z = 2|$  nuclei.

Isotope	$B(E2) \downarrow [e^2 \text{fm}^4]$			
	Expt.	VS-IMSRG	USDB	Ref. (Expt.)
$^{20}\text{Mg}$	35.4 (64)	26.3	37.6	[9]
$^{20}\text{O}$	5.8 (2)	0.9	4.1	[9]
$^{24}\text{Si}$	19.1 (59)	41.4	47.3	[9]
$^{24}\text{Ne}$	28.0 (66)	13.8	40.6	[9]
$^{28}\text{S}$	36.2 (60)	45.1	50.6	[9]
$^{28}\text{Mg}$	67.7 (61)	28.4	63.5	[9]
$^{32}\text{Ar}$	53.7 (139)	37.1	53.5	[9]
$^{32}\text{Si}$	32.0 (91)	21.3	44.5	[9]

FIG. 8.  $B(E2) \downarrow$  values for (top)  $T_z = -\frac{1}{2}$  and (bottom)  $T_z = +\frac{1}{2}$  nuclei. See text for details of the theoretical VS-IMSRG and USDB calculations.FIG. 9.  $B(E2) \downarrow$  values for (top)  $T_z = -1$  and (bottom)  $T_z = +1$  nuclei. See text for details of the theoretical VS-IMSRG and USDB calculations.FIG. 10.  $B(E2) \downarrow$  values for (top)  $T_z = -2$  and (bottom)  $T_z = +2$  nuclei. See text for details of the theoretical VS-IMSRG and USDB calculations.

use of a unitary transformation means that - in principle - no physics is lost in this process. One can then perform configuration interaction calculations within the decoupled model space and capture all physics, even that which might have involved couplings between the core and the external model-space in the original Hamiltonian. The appeal of this method is clear, as it provides a computationally tractable valence-space Hamiltonian without losing physics information from the larger space. It is also necessary to consistently evolve all operators for use in the transformed model-space. This evolution inevitably induces three- and higher-body components, which in practice must be truncated to make the problem tractable. The operator evolution is therefore truncated at the normal-ordered two-body level—the IMSRG(2) approximation—resulting in an inevitable loss of information.

Any disagreement with experiment will be due to one of two sources: deficiencies in the input Hamiltonian (e.g. truncation of the EFT expansion), and truncations in the many-body solution. It is likely that a large fraction of the missing strength in the VS-IMSRG calculations arises from the many-body side (though there will at least be some impact from the small radii). We might expect, however, that the inclusion of two-body elements in the operator evolution will suppress the isovector component of this deficiency. The first-order contribution from out-of-space effects couples an in-space nucleon, with an out-of-space nucleon. Due to the dominance of the  $T = 0$  channel over  $T = 1$  in the interaction, the coupling is strongest between  $np$  pairs. Since the  $E2$  operator couples to the charge of the nucleon, this first-order correction might be expected to predominantly affect out-of-space protons coupling to in-space neutrons, as has been discussed in terms of perturbation theory [26]. These effects are captured by the IMSRG(2) approximation. For higher-order (i.e. 2p-2h excitations and higher), the

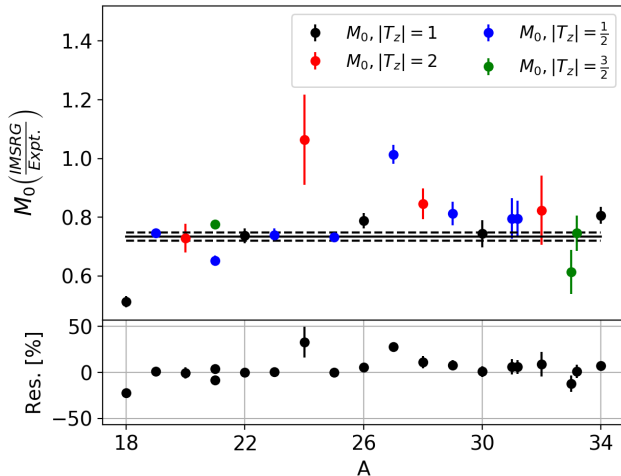


FIG. 11. (Top) Ratio of  $M_0$  calculated from VS-IMSRG calculations and extracted from experimental data for  $sd$ -shell nuclei. A zeroth-order polynomial fit (solid line) is also shown, along with the  $1\sigma$  uncertainties (dashed lines) on the result. The fit yields a deficiency in the VS-IMSRG  $M_0$  value of approximately 75%. (Bottom) Residuals for the fit.

out-of-space couplings become more complex, necessarily involving multiple nucleons and more configurations, meaning any individual isovector coupling contributes less to the ensemble of configurations and yielding an approximately isoscalar net effect.

To investigate this effect, we employ the isoscalar ( $M_0$ ) and isovector ( $M_1$ ) matrix element formalism of Brown et al. [27], where

$$M_0 = \frac{\sqrt{B(E2; T_z < 0)} + \sqrt{B(E2; T_z > 0)}}{2}, \quad (1)$$

and

$$M_1 = \left| \frac{\sqrt{B(E2; T_z < 0)} - \sqrt{B(E2; T_z > 0)}}{\Delta T_z} \right|. \quad (2)$$

Ratios of experimental to theoretical  $M_0$  values are shown in Fig. 11 for the VS-IMSRG calculations and in Fig. 12 for the USDB results. As expected, the VS-IMSRG results underpredict the experimental data, with  $\frac{M_0(\text{IMSRG})}{M_0(\text{Expt.})} \sim 75\%$  on average. By comparison, on average the USDB calculations reproduce  $M_0$  well, with a modest overprediction. Of note is that, while the VS-IMSRG calculations are unable to reproduce the  $M_0$  values, they provide a slightly improved description to the shell-model calculations, as highlighted by the reduced scatter in the residuals shown in the bottom panels of Fig. 11 and Fig. 12. Note, for comparison, that without the use of effective charges the USDB calculations yield  $\frac{M_0(\text{USDB})}{M_0(\text{Expt.})} \sim 55\%$ .

Figure 13 shows the differences between experimental and calculated  $|M_1|$  values for both the VS-IMSRG and

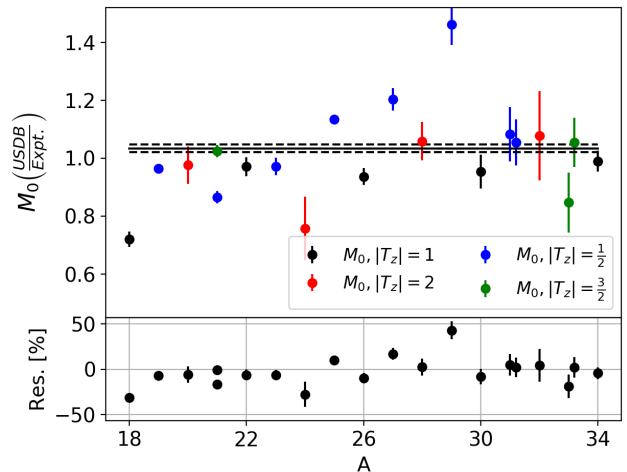


FIG. 12. (Top) Ratio of  $M_0$  calculated from USDB calculations and extracted from experimental data for  $sd$ -shell nuclei. A zeroth-order polynomial fit (solid line) is also shown, along with the  $1\sigma$  uncertainties (dashed lines) on the result. The fit indicates that the USDB  $M_0$  values are approximately consistent with experiment on average, with  $\frac{M_0(\text{USDB})}{M_0(\text{Expt.})} = 1.032(26)$ . (Bottom) Residuals for the fit.

USDB calculations. Both VS-IMSRG and USDB calculations yield, on average,  $|M_1|$  values consistent with experiment. This indicates that, to the level of presently available experimental and theoretical uncertainty, the missing strength in the VS-IMSRG calculations is isoscalar, in line with naïve expectations. In previous work [1] we noted a potential isovector component to the missing VS-IMSRG strength from a study of  $|T_z| = 1$  nuclei. In light of the present, comprehensive study of the  $sd$ -shell, however, we find that this effect is in fact due to a deficiency of isoscalar strength, rather than any excess of isovector.

One can estimate the contribution of the Hamiltonian to the deficiency in isoscalar strength through comparison with charge-radii. As previously mentioned [18] it has been found that VS-IMSRG calculations using the EM1.8/2.0 interaction underpredict charge-radii, with the underprediction being approximately 7%. The corresponding underprediction of the  $E2$  matrix element would then be 13%. Clearly, as shown in Fig. 11, the underprediction in the calculations is larger than can be explained by a deficiency in the Hamiltonian.

To better understand the origin of the consistent underprediction of  $B(E2)$  strengths by the VS-IMSRG calculations, it is therefore informative to remove the ambiguity associated with the input Hamiltonian and consider a case where an exact diagonalization is possible. We therefore performed full configuration interaction (FCI), VS-IMSRG and coupled-cluster (CC, see e.g. Ref. [28]) calculations of  $^{14}\text{C}$ , beginning with the same  $ps\text{-}dmwk$  interaction [29, 30] Hamiltonian in all cases. (The choice of  $^{14}\text{C}$  was made to enable the comparison with coupled-cluster). The FCI calculations were performed in

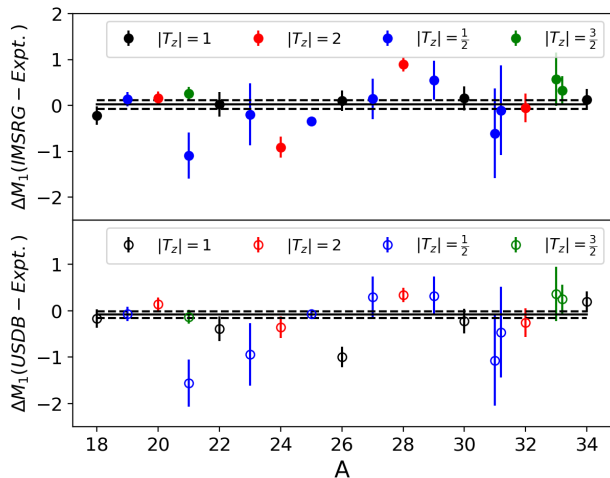


FIG. 13. Differences between experimentally determined  $M_1$  values and those calculated using the VS-IMSRG (top) and shell-model with USDB (bottom). A zeroth-order polynomial fit (solid) line is also shown, along with the  $1\sigma$  uncertainties. Both USDB and VS-IMSRG results are consistent with zero - indicating no missing isovector contribution at the level of the presently achieved uncertainties.

NuShellX. Quadrupole transition amplitudes were therefore determined for protons and neutrons ( $A_p$  and  $A_n$ , respectively) such that

$$B(E2; 2^+ \rightarrow 0^+) = \frac{(A_p \times e_p + A_n \times e_n)^2}{5}, \quad (3)$$

where  $e_p$  and  $e_n$  correspond to the proton and neutron effective charges, respectively. Because we use a Hamiltonian with phenomenologically determined matrix elements, the corresponding radial wave functions are arbitrary. We use a harmonic oscillator basis and present the amplitudes in units of the oscillator length squared  $b^2$ . In the VS-IMSRG calculations, the IMSRG transformation is used to decouple the  $p$ -shell from the  $sd$ -shell, and the resulting  $p$ -shell interaction is diagonalized. In the CC calculations the  $^{14}\text{C}$   $2^+$  excited state is computed using the equation-of-motion coupled-cluster (EOM-CC) formalism [31] which amounts to an expansion in particle-hole excitations out of the CC solution for the  $0^+$  ground state. The order of the expansions used is denoted in parentheses with the first value indicating the highest order ground-state expansion and the second indicating the EOM expansion used to calculate the excited state. Ground-state expansions are CCSD, CCSDT-1 and CCSDT-3, corresponding to singles-doubles, singles-doubles and leading-order triples, and singles-doubles and up to third-order triples [32, 33], respectively. The order of the excited-state expansion is given as S, D or T for 1p-1h, 2p-2h and 3p-3h expansions out of the ground-state, respectively. For example, CC(D/S) corresponds to a CCSD ground-state with the  $2^+$  state expanded in terms of 1p-1h excitations, and CC(T-1/T) corresponds to a CCSDT-1 ground-state with the  $2^+$  state expanded

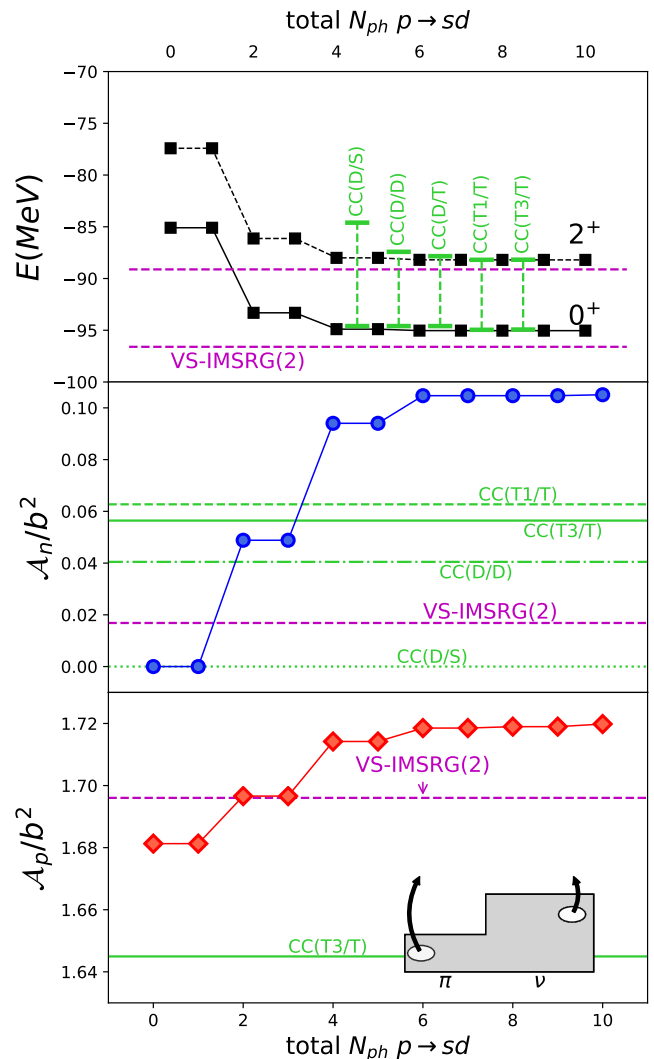


FIG. 14. Absolute  $0_1^+$  and  $2_1^+$  state energies (top row), neutron quadrupole-excitation amplitudes (middle row) and proton quadrupole-excitation amplitudes (bottom row) for  $^{14}\text{C}$  calculated in a full configuration interaction diagonalization with the *psdmw*k interaction, plotted against the number of excitations permitted from the  $p$  to  $sd$  shell. Also shown are the values calculated using the VS-IMSRG method, as well as using an equation-of-motion coupled-cluster methodology. See text for details of calculations.

in terms of excitations up to 3p-3h.

It is found that the FCI ground- and excited state energies are already well reproduced at the EOM-CCSD level and by the VS-IMSRG calculations. On the other hand, we find that the quadrupole amplitudes are consistently underpredicted by VS-IMSRG, consistent with the comparison with experimental data. The EOM-CC calculations show improved reproduction of the FCI interactions with increasing order of expansion, but still significantly underpredict the quadrupole amplitudes even at the CC(T-3/T) order. Since all calculations were per-

formed with the same initial Hamiltonian, this missing strength must arise from the many-body approximation. To further investigate this underprediction, the microscopic behaviour of the configuration interaction was controlled using a series of configuration interaction (CI) calculations, with a truncation on the total number of nucleon excitations out of the  $p$  shell. Figure 14 shows the results of these calculations.

The VS-IMSRG calculations yield an excess of quadrupole amplitude when compared to the fully truncated (i.e.  $p$ -shell only) calculations. This is as expected: the VS-IMSRG evolution attempts to decouple the  $p$  shell from the  $sd$  shell and then diagonalizes within the  $p$  shell, so the amplitude within the  $p$  shell should be completely accounted for. As the truncation conditions are relaxed and excitations into the  $sd$  shell are permitted, the VS-IMSRG calculations soon fail to capture the additional strength, indicating that the SRG-decoupling of the spaces has resulted in information relevant to the quadrupole amplitude being lost. The CC calculations do not fully reproduce the pure  $p$ -shell amplitude for the open-shell protons (bottom panel, Fig. 14). Perhaps more interestingly, however, is a comparison to the closed-shell neutrons (middle panel, Fig. 14). Increasing the order of the CC-EOM calculations - effectively allowing for correlated 3p-3h excitations, in the case of CC(T/T) - clearly helps restore missing strength. Due to the exponential ansatz, the CC wavefunctions at CC(T/T) contain a fraction of up to 6p-6h excitations, however these excitations are limited to disconnected 6p-6h cluster terms, i.e. products of lower rank excitations. The fact that the quadrupole amplitudes remain deficient even at the CC(T/T) level implies that connected 4p-4h and higher excitations are required to reproduce the amplitude.

## V. CONCLUSIONS

$^{23}\text{Mg}$  and  $^{23}\text{Na}$  have been studied by Coulomb excitation using particle- $\gamma$  coincidences at TRIUMF-ISAC. The relative insensitivity of the Coulomb excitation methodology to the  $M1$  transitions which dominate the decay of the first excited states allowed for the extraction of  $E2$  transition strengths with superior precision to that previously achieved, while agreeing within uncertainties with literature values. Calculations were performed, employing both the shell-model with the USDB interaction, and the *ab initio* valence-space in-medium similarity renormalization group methodology.

Consistent with previous work, it was found that the VS-IMSRG calculations significantly underpredict the

$E2$  transition strength. This underprediction must arise from the two-body truncation to the operator evolution applied to make the method computationally tractable. A comprehensive survey of the literature in combination with the present work was performed and compared with the VS-IMSRG and shell-model results. It is found that the missing strength is predominantly isoscalar in nature, while the isovector contribution is consistent with zero within presently available experimental and theoretical uncertainties. We provided a brief discussion on the VS-IMSRG calculations, presenting a potential explanation for the apparent lack of isovector contribution to the missing  $E2$  strength.

Finally, full- and truncated-configuration interaction calculations of  $^{14}\text{C}$  were performed and compared with both VS-IMSRG and coupled-cluster calculations. These calculations indicate that high-order connected particle-hole excitations may play a significant role in quadrupole transitions amplitudes, and we emphasize that even if energetics are accurately reproduced, transitions amplitudes might be much more sensitive to fine details in the wavefunction that can not be captured at a low-order truncation level.

## VI. ACKNOWLEDGEMENTS

The authors would like to thank the TRIUMF beam delivery group for their efforts in providing high-quality stable and radioactive beams. This work has been supported by the Natural Sciences and Engineering Research Council of Canada (NSERC), The Canada Foundation for Innovation and the British Columbia Knowledge Development Fund. TRIUMF receives federal funding via a contribution agreement through the National Research Council of Canada. Computations were performed with an allocation of computing resources on Cedar at West-Grid and Compute Canada, and on the Oak Cluster at TRIUMF managed by the University of British Columbia department of Advanced Research Computing (ARC). Work at LLNL was performed under contract DE-AC52-07NA27344. This work was supported by the Office of Nuclear Physics, U.S. Department of Energy, under grants desc0018223 (NUCLEI SciDAC-4 collaboration) and by the Field Work Proposal ERKBP72 at Oak Ridge National Laboratory (ORNL). SRS is supported by the U.S. Department of Energy under contract DE-FG02-97ER41014.

Fig. 5 was created using the SciDraw scientific figure preparation system [34]. The codes `imsrg++` [35] and `nutbar` [23] used in this work make use of the Armadillo library [36].

---

[1] J. Henderson, G. Hackman, P. Ruotsalainen, S. Stroberg, K. Launey, J. Holt, F. Ali, N. Bernier, M. Bentley,

M. Bowry, R. Caballero-Folch, L. Evitts, R. Frederick, A. Garnsworthy, P. Garrett, B. Jigmeddorj, A. Kilic,

- J. Lassen, J. Measures, D. Muecher, B. Olaizola, E. O'Sullivan, O. Paetkau, J. Park, J. Smallcombe, C. Svensson, R. Wadsworth, and C. Wu, *Physics Letters B* **782**, 468 (2018).
- [2] G. Hackman and C. E. Svensson, *Hyperfine Int.* **225**, 241 (2014).
- [3] S. Raeder, H. Heggen, J. Lassen, F. Ames, D. Bishop, P. Bricault, P. Kunz, A. Mjøs, and A. Teigelhofer, *Rev. Sci. Instr.* **85**, 033309 (2014).
- [4] K. Jayamanna, F. Ames, G. Cojocar, R. Baartman, P. Bricault, R. Dube, R. Laxdal, M. Marchetto, M. MacDonald, P. Schmor, G. Wight, and D. Yuan, *Review of Scientific Instruments* **79**, 2 (2008).
- [5] "GRSISort," <https://github.com/GRIFFINCollaboration/GRSISort> ().
- [6] R. Brun and F. Rademakers, *Nucl. Instr. Meth. in Phys. Res. A* **389**, 81 (1997).
- [7] T. Czornyka, D. Cline, and C. Y. Wu, *Bull. Am. Phys. Soc.* **28**, 745 (1983).
- [8] N. J. Stone, *Atomic Data and Nuclear Data Tables* **90**, 75 (2005).
- [9] NNDC, "Evaluated Nuclear Structure Data File (ENSDF)."
- [10] K. Tsukiyama, S. K. Bogner, and A. Schwenk, *Phys. Rev. C* **85**, 061304(R) (2012).
- [11] S. K. Bogner, H. Hergert, J. D. Holt, A. Schwenk, S. Binder, A. Calci, J. Langhammer, and R. Roth, *Phys. Rev. Lett.* **113**, 142501 (2014).
- [12] S. R. Stroberg, A. Calci, H. Hergert, J. D. Holt, S. K. Bogner, R. Roth, and A. Schwenk, *Phys. Rev. Lett.* **118**, 032502 (2017).
- [13] S. R. Stroberg, S. K. Bogner, H. Hergert, and J. D. Holt, *Ann. Rev. Nucl. Part. Sci.* **69**, 307 (2019).
- [14] K. Hebeler, S. K. Bogner, R. J. Furnstahl, A. Nogga, and A. Schwenk, *Phys. Rev. C* **83**, 031301 (2011).
- [15] J. Simonis, K. Hebeler, J. D. Holt, J. Menéndez, and A. Schwenk, *Phys. Rev. C* **93**, 011302(R) (2016).
- [16] S. K. Bogner, R. J. Furnstahl, and R. J. Perry, *Phys. Rev. C* **75**, 061001 (2007).
- [17] D. R. Entem and R. Machleidt, *Phys. Rev. C* **68**, 041001 (2003).
- [18] J. Simonis, S. R. Stroberg, K. Hebeler, J. D. Holt, and A. Schwenk, *Phys. Rev. C* **96**, 014303 (2017).
- [19] T. D. Morris, J. Simonis, S. R. Stroberg, C. Stumpf, G. Hagen, J. D. Holt, G. R. Jansen, T. Papenbrock, R. Roth, and A. Schwenk, *Phys. Rev. Lett.* **120**, 152503 (2018).
- [20] J. D. Holt, S. R. Stroberg, A. Schwenk, and J. Simonis, (2019), [arXiv:1905.10475](https://arxiv.org/abs/1905.10475).
- [21] B. A. Brown and W. A. Richter, *Phys. Rev. C* **74**, 034315 (2006).
- [22] B. A. Brown and W. D. M. Rae, *Nucl. Data Sheets* **120**, 115 (2014).
- [23] <https://github.com/ragnarstroberg/nutbar> ().
- [24] P. Ruotsalainen, J. Henderson, G. Hackman, G. H. Sargsyan, K. D. Launey, A. Saxena, P. C. Srivastava, S. R. Stroberg, T. Grahn, J. Pakarinen, R. Julin, P. T. Greenlees, J. Smallcombe, C. Andreoiu, G. C. Ball, S. Bert, M. Bernier, M. Bowry, M. Buckner, R. Caballero-Folch, A. Chester, S. Cruz, L. J. Evitts, R. Frederick, A. B. Garnsworthy, M. Holl, A. Kurkjian, D. Kisliuk, K. G. Leach, E. McGee, J. Measures, D. Muecher, J. Park, F. Sarazin, J. K. Smith, D. Southall, K. Starosta, C. E. Svensson, K. Whitmore, M. Williams, and C. Y. Wu, *Physical Review C* **99**, 051301(R) (2019).
- [25] J. M. VonMoss, S. L. Tabor, V. Tripathi, A. Volya, B. Abromeit, P. C. Bender, D. D. Caussyn, R. Dungan, K. Kravvaris, M. P. Kuchera, R. Lubna, S. Miller, J. J. Parker, and P.-L. Tai, *Phys. Rev. C* **92**, 034301 (2015).
- [26] S. Siegel and L. Zamick, *Nuclear Physics A* **145**, 89 (1970).
- [27] B. A. Brown, B. H. Wildenthal, W. Chung, S. E. Massen, M. Bernas, A. M. Bernstein, R. Miskimen, V. R. Brown, and V. A. Madsen, *Phys. Rev. C* **26**, 2247 (1982).
- [28] G. Hagen, T. Papenbrock, M. Hjorth-Jensen, and D. J. Dean, *Rep. Prog. Phys.* **77**, 096302 (2014).
- [29] E. K. Warburton and B. A. Brown, *Physical Review C* **46**, 923 (1992).
- [30] E. K. Warburton, B. A. Brown, and D. J. Millener, *Physics Letters B* **293**, 7 (1992).
- [31] J. F. Stanton and R. J. Bartlett, *J. Chem. Phys.* **98**, 7029 (1993).
- [32] Y. S. Lee, S. A. Kucharski, and R. J. Bartlett, *Journal of Chemical Physics* **81**, 5906 (1984).
- [33] J. D. Watts and R. J. Bartlett, *Chemical Physics Letters* **258**, 581 (1996).
- [34] M. Caprio, *Comput. Phys. Commun.* **107**, 171 (2005).
- [35] <https://github.com/ragnarstroberg/imsrg> ().
- [36] C. Sanderson, Technical Report, NICTA (2010).